



High resolution transmission electron microscopy and molecular simulation analysis of ϵ -Fe_{2.3}N and γ' -Fe₄N formation for a nitrated 4140 steel

Luis Béjar^a, Ariosto Medina-Flores^{b,c}, Ismeli Alfonso^{b,✉}, Héctor Carreón^a, José Solís^c

^aUniversidad Michoacana de San Nicolás de Hidalgo (UMSNH),
Ciudad Universitaria, 58000, Morelia, Michoacán, México

^bInstituto de Investigaciones en Materiales. Universidad Nacional Autónoma de México, Circuito
Exterior s/n, Ciudad Universitaria. CP 04510. Del. Coyoacán, México DF. México

^cSEP-DGEST-IT de Tlalnepantla, Av. Tecnológico s/n, Col. La Comunidad, Tlalnepantla de Báez, Edo México, 54070, México

✉Corresponding author: ialfonso@unam.mx

Submitted: 13 April 2014; Accepted: 26 February 2015; Available On-line: 14 May 2015

ABSTRACT: High Resolution Transmission Electron Microscopy (HRTEM) and molecular simulation techniques were applied to analyze phase formation in the post-discharge microwave nitriding process of a 4140 steel. The results showed the formation of ϵ -Fe_{2.3}N and γ' -Fe₄N. The morphology of the γ' -Fe₄N phase was composed by cubic nanoparticles that grows in the $\langle 0\ 0\ 1 \rangle$ axis direction. Otherwise, the ϵ -Fe_{2.3}N crystal is associated to hexagonal faces in the $[0\ 0\ 1]$ direction which grows forming angles of 120°. The comparison between experimental and analytical results allowed a better understanding of the phases formed during this nitriding process.

KEYWORDS: HRTEM; Morphology; Nitriding; Phases; Simulation

Citation / Cómo citar este artículo: Béjar, L., Medina-Flores, A., Alfonso, I., Carreón, H., Solís, J. (2015) "High resolution transmission electron microscopy and molecular simulation analysis of ϵ -Fe_{2.3}N and γ' -Fe₄N formation for a nitrated 4140 steel". *Rev. Metal.* 51(2): e041. doi: <http://dx.doi.org/10.3989/revmetalm.041>.

RESUMEN: Análisis mediante microscopía electrónica de transmisión de alta resolución y simulación molecular de la formación de las fases ϵ -Fe_{2.3}N y γ' -Fe₄N en un acero 4140 nitrurado. Se utilizaron técnicas de Microscopía Electrónica de Transmisión de Alta Resolución (MET AR) y de simulación molecular para analizar la formación de fases en el proceso de nitruración por descargas de microondas de un acero 4140. Los resultados mostraron la formación de las fases ϵ -Fe_{2.3}N y γ' -Fe₄N. Se observó que la fase γ' -Fe₄N está compuesta por nanopartículas cúbicas que crecen en la dirección $\langle 0\ 0\ 1 \rangle$. Por otra parte, la fase ϵ -Fe_{2.3}N está asociada con caras hexagonales en la dirección $[0\ 0\ 1]$, las cuales crecen formando ángulos de 120° entre sí. La comparación entre los resultados experimentales y analíticos permitieron una mejor comprensión de las fases formadas durante este proceso de nitruración.

PALABRAS CLAVE: Fases; MET; Morfología; Nitruración; Simulación

Copyright: © 2015 CSIC. This is an open-access article distributed under the terms of the Creative Commons Attribution-Non Commercial (by-nc) Spain 3.0 License.

1. INTRODUCTION

Structural steel and components used in severe environments must have excellent fatigue and wear resistance. Consequently, their surfaces should be modified to provide high hardness values to resist

wear, while the inner cores still need to have high toughness strength. The positive effects of surface treatments, like nitriding, on the fatigue and wear properties, have been known for several decades, as shown by Xi *et al.* (2008). During this treatment a nitride layer is formed, composed by ϵ -Fe_{2.3}N and

γ -Fe₄N which are responsible to enhance mechanical properties. In this sense, the nitrided layers have been studied by several characterization techniques. Medina-Flores *et al.* (2004) used scanning electron microscopy (SEM), energy dispersive spectrometry (EDS), x-ray diffraction (XRD) and high resolution transmission electron microscopy (HRTEM). Shoaib *et al.* (2008) characterized surface properties by using XRD and Vickers microhardness. Salas *et al.* (1996) used SEM and optical microscopy, also analyzing cross sections; while Corengia *et al.* (2005) used electron probe microanalysis (EPMA) and atomic force microscopy (AFM) for the study of topographical evolution and roughness of the nitrided layer. These studies emphasize characteristics such as composition, structure, morphology and chemical properties. On the other hand, molecular simulation techniques have gained strength amongst the scientific community during the last two decades, for molecular or crystal systems, by classical and quantum mechanism approximations. Computational materials science has been used as a virtual laboratory for the analysis of the nitriding process. Ratajski and Suszko (2008) developed a model of the nitriding process, simulating the growth kinetics in the nitrided layers, as well as the calculation of nitrogen profiles in the diffusion layer. Ju *et al.* (2003) proposed a numerical model when considering quantitative effects of diffused carbon and nitrogen gradients and kinetics of phase transformation, successfully predicting the profiles of nitrogen as well as residual stresses and distortions after nitriding.

Other studies were focused on electronic structure, charge distribution and atomic configuration, analyzing the mechanism behind the unusual behavior of nitride compounds and the valence alteration or nitrogen-induced charge polarization and transportation, which takes the responsibility for the high corrosion and wear resistant of nitrides, like the work of Zheng and Sun (2006). Pietrzyk *et al.* (1996) used finite element analysis for the study of kinetics during nitriding process. Guechichi and Castex (2006), predicted the fatigue limit for cyclical loading of surface treated materials, including nitriding. In this sense, it is important a comparison between theoretical and experimental data, emphasizing in the importance of computations in materials science, an important tool for an easier interpretation and identification of small details of the materials (Al Omar and Prado, 2010).

One of the most used techniques for nitriding layer and nanoparticles characterization is HRTEM. The interpretation of the images obtained using this technique helps to determine the structure and composition of local crystalline nanoparticles arrangements, as the work of Yacaman *et al.* (1999), who characterized nanoparticles embedded in different matrices using HRTEM. Ascencio *et al.* (1998) found that the combination of HRTEM

experimental and theoretical analysis is very useful for obtaining the full characterization of nanoparticles. For the nitriding process a conjugated study like the above mentioned could be very interesting for a better understanding of the process. In this work, we report the results obtained by X-Ray diffraction, HRTEM analysis, molecular and HRTEM simulation for a 4140 steel, nitrided by the post-discharge microwave method. Experimental and theoretical data were compared in order to have a well-supported interpretation of the experimental results, mainly for the growth of the nitrides formed during the nitriding treatment.

2. MATERIALS AND METHODS

2.1. Experimental

Rectangular specimens (10×20×20 mm) were cut from an AISI SAE 4140 steel bar with a composition (in wt.%) of 0.412 C, 0.665 Mn, 0.23 Si, 0.015 P, 0.014 S, 1.15 Cr, 0.15 Mo and 0.50 Ni. The specimen surface to be exposed was polished and thoroughly cleaned in an acetone ultrasonic bath before nitriding. After preparation, the specimens were introduced into a tubular resistance furnace in an Ar-H₂ post-discharge flow, and heated to 810 K and 850 Pa. Once the nitriding temperature was reached, the gas mixture was switched to 40 sccm of N₂, 4 sccm of Ar and 100 sccm of H₂ during 15 minutes. Then the samples were slowly cooled in the reactor under an Ar atmosphere. In order to compare the simulated models with actual experimental results, the nitrided samples were analyzed using a Siemens D5000 X-ray diffractometer equipped with graphite monochromatized high intensity CuK λ ($\lambda=0.154178$ nm). The Bragg angle 2θ ranges from 20° to 100° at a scanning rate of 0.06 °C s⁻¹. HRTEM images were captured using a TEM FEG FEI TECNAI F20 at Scherzer conditions (well established by Williams and Carter, 1996) with an acceleration voltage of 200 kV, a spherical aberration of Cs=1 mm and a point resolution of ≈ 1.6 Å. Thin foils for HRTEM investigations were prepared by sectioning off the nitriding layer with a low speed saw. The samples were then mechanically polished, followed by ion milling. The final ion-milling step was performed at grazing incidence to avoid preferential sputtering of one nitride specie over the others. The HRTEM images were digitalized using a SensysColor low noise CCD. The fast fourier transform (FFT) of the digital images was obtained by applying frequency filters to reduce the noise and to enhance their structures.

2.2. Computer simulation

The crystals models were built based on the data of Table 1, where the crystalline lattice, space group, cell dimension, angles and fundamental positions

TABLE 1. Unit cell data used for the quantum calculations (Jack, 1951)

Crystal	Crystal lattice	Space group	Cell vectors	Cell angles	Fundamental positions
ϵ -Fe _{2.3} N	HCP	P 6	a=b=2.695 Å	$\alpha=\beta=90^\circ$	Fe (0 2/3 1/4)
			c=4.362 Å	$\gamma=120^\circ$	Fe (1/3 1/3 1/4)
					Fe (2/3 0 1/4)
					Fe (1/3 0 3/4)
					Fe (0 1/3 3/4)
					Fe (2/3 2/3 3/4)
γ -Fe ₄ N	FCC	F d-3	a=3.795 Å	$\alpha=90^\circ$	N (1/3 2/3 1/2)
					N (2/3 1/3 0)
					Fe (0 0 0)
					Fe (1/2 0 1/2)
					Fe (1/2 1/2 0)
					Fe (0 1/2 1/2)
				N (1/2 1/2 1/2)	

are summarized for each unit cell. Focusing on a full characterization of the ϵ -Fe_{2.3}N and γ -Fe₄N nitrides, crystal diffraction, morphology and HRTEM image models were calculated using the Cerius 2 software. Conditions were simulated at 200 kV, TEM voltage used in the experimental analysis. The images were calculated for a 5×5×5 unit cell model in the [0 0 1] orientation.

3. RESULTS AND DISCUSSION

The specimen composition and microstructure become very important parameters due to their significant contribution to the macroscopic properties. The phases of the untreated and nitrated samples and their crystallographic orientations were identified by XRD measurements. Figure 1a shows an X-ray diffraction pattern of the untreated sample. It can be observed that all the peaks correspond to the α -Fe crystal; while in Fig. 1b, which corresponds to the nitride sample, two main phases were recognized: ϵ -Fe_{2.3}N and γ -Fe₄N. No other phases peaks were detected.

Figure 2 shows the simulated X-ray diffractograms for: (a) α -Fe phase, (b) γ -Fe₄N and (c) ϵ -Fe_{2.3}N nitrides respectively. All patterns show the main peaks of the corresponding phases which aim to compare directly to the obtained experimental data. In the simulated diffractograms the crystal is considered pure because of the absence of noise produced for the surrounding material. This fact allows obtaining a clear quantity of detectable peaks with higher intensities compared to the experimental results.

In order to understand the growth of the nitrides three of the main analytical data parameters were calculated: crystal model, crystalline morphology and HRTEM simulated image. Figures 3 and 4 show images and different analyses for the produced

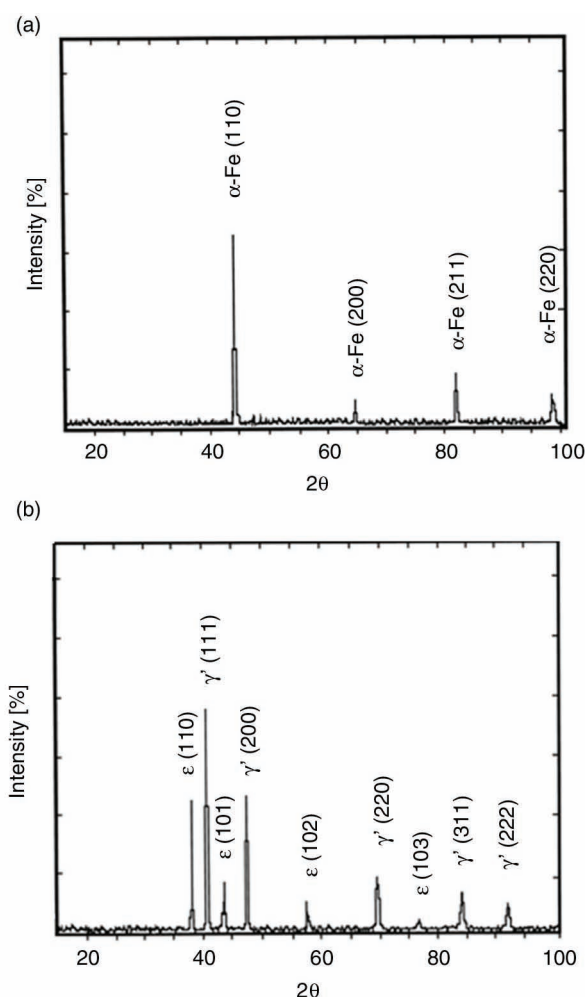


FIGURE 1. X-ray diffractograms of: the untreated (a) and nitrated (b) samples showing the presence of peaks corresponding to α -Fe for the untreated sample and ϵ -Fe_{2.3}N and γ -Fe₄N for the nitrated one.

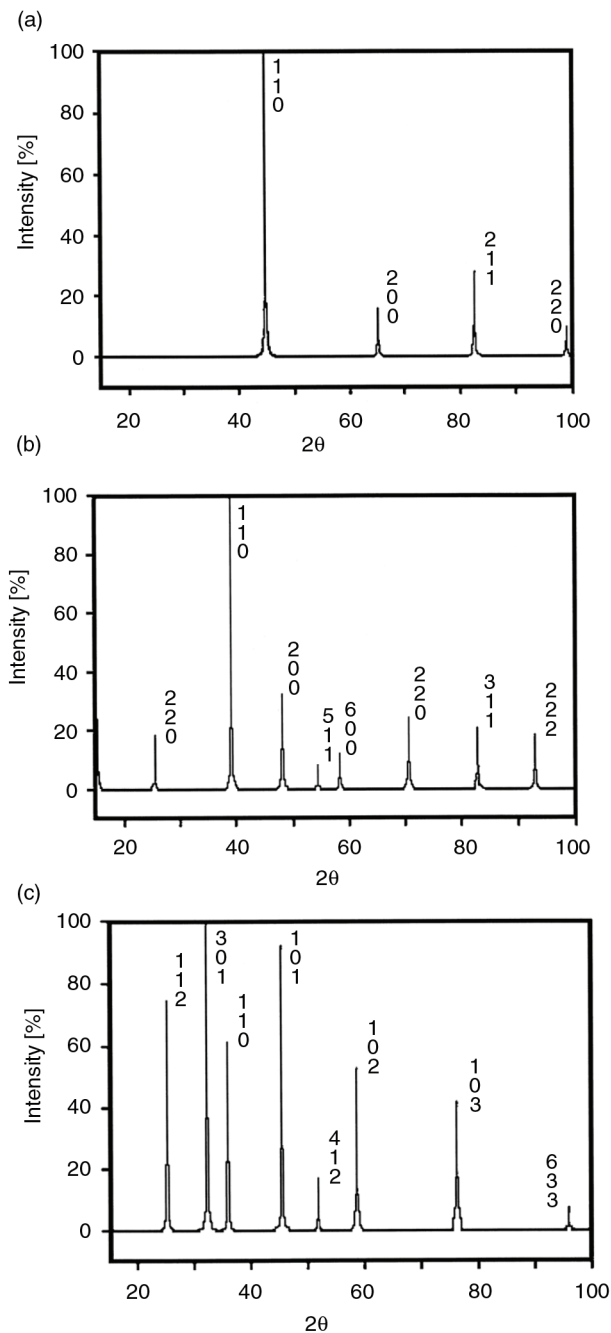


FIGURE 2. Simulated X-ray diffractograms for: (a) α -Fe, (b) γ' -Fe₄N and (c) ϵ -Fe_{2.3}N.

nitrides. Figure 3a presents the crystal model for the ϵ -Fe_{2.3}N nitride in the [0 0 1] orientation. It is possible to observe an hexagonal lattice over the a-b cell planes where six N atoms are around of a Fe central atom forming hexagons. Figure 3b shows the crystalline morphology. Hexagonal faces in the $\langle 0 0 1 \rangle$ axis direction determine the ϵ -Fe_{2.3}N crystal habit. It is possible to observe that the ϵ -Fe_{2.3}N nitride will produce flat faces with angles of 120° and 90°

between them. Figure 3c shows the experimental HRTEM image for the ϵ -Fe_{2.3}N phase obtained during the nitriding treatment. A nanoparticle with hexagonal shape morphology can be observed, which directly match to the theoretical calculations. The FFT of the ϵ -Fe_{2.3}N nitride with the (001) plane indexed is showed in the Fig. 3d. The Figure 3e shows the Inverse FFT (IFFT) filtered image in which can be observed that the nanoparticle is formed for hexagons matching with the theoretically calculated results. Figure 3f shows the simulated model along the [0 0 1] axes which match with experimental image of the Fig. 3c.

Figure 4a presents the crystal model for γ' -Fe₄N nitrides in the [0 0 1] orientation where is it possible to observe a regular distribution of Fe and N atoms in two dimensions. The corresponding morphology of the γ' -Fe₄N nitride is observed in Fig. 4b, where the γ' -Fe₄N nitride is clearly characterized by a cubic fiber shape with square faces that grows in the $\langle 0 0 1 \rangle$ axis direction. It is clear that the growing shape produces fibers and flat surfaces with angles of 90° and 45° between their planes. Figure 4c shows the experimental HRTEM image with a well-defined contrast, characteristic of the γ' -Fe₄N phase. It is possible to observe that the nitride grows following a fiber-like morphology. Figure 4d presents the FFT of this phase, which is related to the electron diffraction pattern. It can determined that the image also corresponds to an orientation near to the [0 0 1] axis, with a FCC structure. The cubic patterns expected from this axis and structure are observed in Fig. 4c, matching with the filtered image and simulated model: Fig. 4e and 4f, respectively. Figure 4e presents the filtered image, indicating a distance between parallel atomic planes of 0.268 nm and 0.189 nm. It is possible to observe lines at 90° to each other with similar distances between them, which correspond directly to the theoretically data calculated for this phase. Figure 4f shows the simulated model along the [0 0 1] axes which match with the experimental image of the Fig. 4e.

4. CONCLUSIONS

- From the analysis presented in this work, we have proved the possibility to compare experimental results versus analytical results, which will allow a better understanding of ϵ -Fe_{2.3}N and γ' -Fe₄N formation during nitriding. A direct observation and a full digital process based on frequency filtering and simulation tools is shown for obtaining distinguishable parameters of two different phases of crystals with near-lattice parameters.
- Digital and HRTEM simulation methods allowed distinguishing the different structures, using local information with small differences in contrast and lattice spacing, which implies

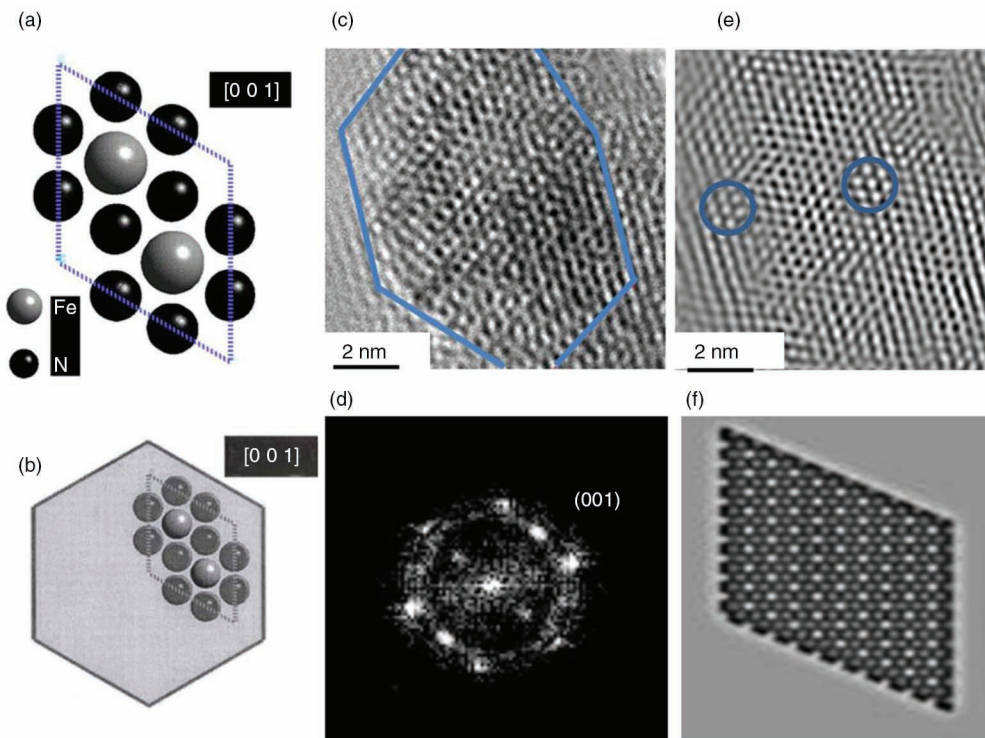


FIGURE 3. (a) Crystals models for the ϵ -Fe_{2.3}N nitride in [0 0 1] orientation, (b) calculated morphology for ϵ -Fe_{2.3}N nitride in [0 0 1] orientation, (c) experimental HRTEM image of ϵ -Fe_{2.3}N nitride showing a nanoparticle with hexagonal morphology, (d) FFT image in the (0 0 1) plane, (e) the processed image showing an hexagonal arrangement and (f) simulated image along the [0 0 1] axes.

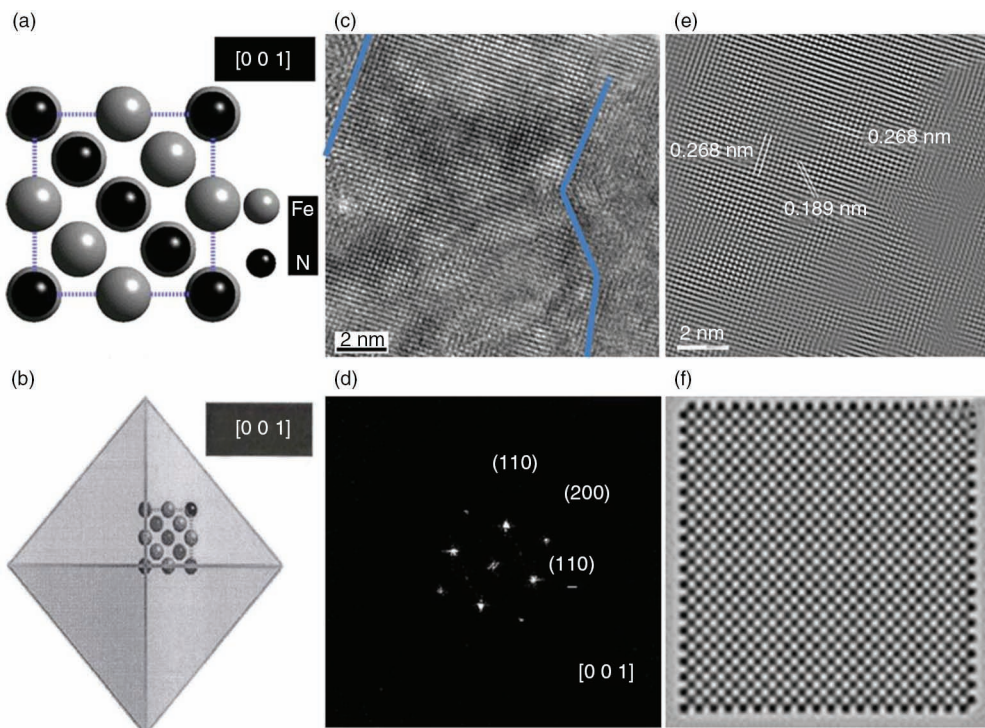


FIGURE 4. (a) Crystal model for the γ' -Fe₄N nitride in [0 0 1] orientation, (b) calculated morphology for γ' -Fe₄N in [0 0 1] orientation, (c) experimental HRTEM image of γ' -Fe₄N nanoparticle with fiber morphology, (d) FFT image in the [0 0 1] axes, (e) processed image showing a FCC arrangement with different atomic planes and (f) simulated image along the [0 0 1] axes.

a complicated problem that is not possible to be solved by means of the X-ray diffractogram patterns.

- Analytical, molecular and simulation methods provide the basis for further analysis in the nitriding materials involved in this work, which open a wide range of possibilities for a better understanding of the materials manipulation and the focusing effort to the materials designers for predicting the kind of growing and morphology during the nitriding treatment. Besides, experimental and theoretical contrast clearly math, corroborating the exactitude of the used models.
- These results can help to provide a full and easier characterization by means of a direct comparison between experimental and theoretical images with different orientations.

REFERENCES

- Al Omar, A., Prado, J.M. (2010). Criterios de predicción de inestabilidades plásticas en procesos de conformado en caliente. (Parte I: Revisión teórica). *Rev. Metal.* 46 (2), 143–161. <http://dx.doi.org/10.3989/revmetalm.0935>.
- Ascencio, J.A., Gutiérrez-Wing, C., Espinoza, M.E., Marin, M., Tehuacanero, S., Zorrilla, C., José-Yacamán, M. (1998). Structure determination of small particles by HREM imaging: theory and experiment. *Surf. Sci.* 396 (1–3), 349–368. [http://dx.doi.org/10.1016/S0039-6028\(97\)00689-4](http://dx.doi.org/10.1016/S0039-6028(97)00689-4).
- Corengia, P., Ybarra, G., Moina, C., Cabo, A., Broitman, E. (2005). Microstructural and topographical studies of DC-pulsed plasma nitrided AISI 4140 low-alloy steel. *Surf. Coat. Tech.* 200 (7), 2391–2397. <http://dx.doi.org/10.1016/j.surfcoat.2005.01.060>.
- Guechichi, H., Castex, L. (2006). Fatigue limits prediction of surface treated materials. *J. Mater. Process. Tech.* 172 (3), 381–387. <http://dx.doi.org/10.1016/j.jmatprotec.2005.10.010>.
- Jack, K.H. (1951). The Occurrence and the Crystal Structure of alpha -Iron Nitride; a New Type of Interstitial Alloy Formed during the Tempering of Nitrogen-Martensite. *Proc. Roy. Soc. London. Ser. A* 208, 216–224. <http://dx.doi.org/10.1098/rspa.1951.0155>.
- Ju, D.Y., Liu, C., Inoue, T. (2003). Numerical modeling and simulation of carburized and nitrided quenching process. *J. Mater. Process. Tech.* 143–144, 880–885. [http://dx.doi.org/10.1016/S0924-0136\(03\)00378-9](http://dx.doi.org/10.1016/S0924-0136(03)00378-9).
- Medina-Flores, A., Oseguera, J., Santiago, P., Ascencio, J.A. (2004). Structural analysis of AISI-SAE 4140 steel nitrided by post-discharge microwave. *Surf. Coat. Tech.* 188–189, 7–12. <http://dx.doi.org/10.1016/j.surfcoat.2004.07.092>.
- Pietrzyk, M., Kryzhanovski, M., Okara, S., Parchomenko, V. (1996). Thermal-diffusion finite element analysis of nitriding process for arc plasma surface hardening of steel. *J. Mater. Process. Tech.* 56 (1–4), 412–421. [http://dx.doi.org/10.1016/S0924-0136\(95\)01855-7](http://dx.doi.org/10.1016/S0924-0136(95)01855-7).
- Ratajski, J., Suszko, T. (2008). Modelling of the nitriding process. *J. Mater. Process. Tech.* 195 (1–3), 212–217. <http://dx.doi.org/10.1016/j.jmatprotec.2007.04.133>.
- Salas, O., Figueroa, U., Palacios, M., Oseguera, J. (1996). Mechanisms of phase formation during post-discharge nitriding. *Surf. Coat. Tech.* 86–87, 332–337. [http://dx.doi.org/10.1016/S0257-8972\(96\)03036-8](http://dx.doi.org/10.1016/S0257-8972(96)03036-8).
- Shoaib Shaha, M., Saleem, M., Ahmad, R., Zakaullah, M., Qayyuma, A., Murtaza, G. (2008). Langmuir probe characterization of nitrogen plasma for surface nitriding of AISI-4140 steel. *J. Mater. Process. Tech.* 199 (1–3), 363–368. <http://dx.doi.org/10.1016/j.jmatprotec.2007.08.025>.
- Williams, D.B., Carter, C.B. (1996). *Transmission Electron Microscopy: A Textbook for Materials Science*, Plenum Press, New York.
- Xi, Y.T., Liu, D.X., Han, D., Han, Z.F. (2008). Improvement of mechanical properties of martensitic stainless steel by plasma nitriding at low temperature. *Acta. Metall. Sin.* 21 (1), 21–29. [http://dx.doi.org/10.1016/S1006-7191\(08\)60015-0](http://dx.doi.org/10.1016/S1006-7191(08)60015-0).
- Yacamán, M.J., Zorrilla, C., Ascencio, J.A., Mondragón, G., Reyes-Gasga, J. (1999). Study of High Resolution TEM Images of Nanoparticles either Supported on Amorphous Films or Embedded in a Crystalline Matrix. *Mater. Trans. JIM* 40 (2), 141–145. <http://www.jim.or.jp/journal/e/40/02/141.html>.
- Zheng, W.T., Sun, Ch.Q. (2006). Electronic process of nitriding: Mechanism and applications. *Prog. Solid State. Ch.* 34 (1), 1–20. <http://dx.doi.org/10.1016/j.progsolidstchem.2005.12.001>.